Published in final edited form as:
Nucl Med Biol. 2012 October ; 39(7): 1012–1018. doi:10.1016/j.nucmedbio.2012.05.006.

A simplified synthesis of the hypoxia imaging agent 2-(2-Nitro-1*H*-imidazol-1-yl)-*N*-(2,2,3,3,3-[^{18}F]pentafluoropropyl)-acetamide ([^{18}F]EF5)

Satish K. Chitneni[a,*], **Gerald T. Bida**[a,*], **Mark W. Dewhirst**[b], and **Michael R. Zalutsky**[a,b]
[a]Department of Radiology, Duke University Medical Center, Durham, NC 27710, USA
[b]Department of Radiation Oncology, Duke University Medical Center, Durham, NC 27710, USA

Abstract

Introduction—[^{18}F]EF5 is a validated marker for PET imaging of tumor hypoxia. It is prepared by reacting a trifluoroallyl precursor with carrier-added [^{18}F]F_2 gas in trifluoroacetic acid (TFA) solvent. We report here an improved radiosynthesis and purification of [^{18}F]EF5 by utilizing an electroformed nickel (Ni) target for [^{18}F] F_2 production, and Oasis® HLB cartridges for on-line solid phase extraction of [^{18}F]EF5 prior to HPLC purification.

Methods—[^{18}F]F_2 was produced by deuteron bombardment of neon plus F_2 in an Ni target, and bubbled through the radiolabelling precursor solution. Purification was achieved by extracting the contents of the crude reaction mixture onto Oasis HLB cartridges, and subsequently eluted onto a semi-preparative HPLC column for further separation. Purified [^{18}F]EF5 was evaluated in small animal PET studies using HCT116 tumor xenografts in nude mice.

Results—The electroformed Ni target enabled recovery of >75% of the radioactivity from the cyclotron target, resulting in 16.2±2.2 GBq (438±58 mCi) of [^{18}F]F_2 available for the synthesis. Use of Oasis cartridges yielded a less complex mixture for purification. On average, 1140±200 MBq (30.8±5.4 mCi) of [^{18}F]EF5 were collected at EOS. Small animal PET imaging studies showed specific retention of [^{18}F]EF5 in tumors, with tumor-to-muscle ratios of 2.7±0.3 at about 160 min after injection.

Conclusion—A simple procedure has been developed for the routine synthesis of [^{18}F]EF5 in amounts and purity required for clinical studies. This new method avoids the need for TFA evaporation and also enables facile automation of the synthesis using commercially available radiosynthesis modules.

Keywords

Hypoxia; PET; [^{18}F]EF5; Oasis® cartridge; On-line SPE

1. Introduction

Solid tumors contain regions with low oxygen concentration, also known as hypoxia [1,2]. Hypoxia causes genomic changes by upregulation of the transcription factor hypoxia inducible factor 1 (HIF-1) and can promote tumor invasiveness and metastasis [3–7]. Additionally, it leads to decreased sensitivity of tumors to radiation therapy and

*Corresponding authors. S.K. Chitneni is to be contacted at: Tel.: +1 919 684 7809; G.T. Bida: Tel.: +1 919 684 7704; fax: +1 919 684 7122. satish.chitneni@dm.duke.edu (S.K. Chitneni), jerry.bida@duke.edu (G.T. Bida).

chemotherapy. Hypoxia results in inefficient transformation of therapeutic radiation induced damage to cytotoxic DNA-strand breaks [8]. The effectiveness of chemotherapy is diminished by limited drug diffusion to hypoxic tumor regions [9] and through activation of multiple molecular mechanisms that decrease the sensitivity of (hypoxic) tumor cells to anti-cancer drugs [10–12]. Because of these potential effects of hypoxia on tumor biology and therapy, monitoring tumor hypoxia status could provide a valuable tool for treatment planning. Several different methods are in use for the detection and measurement of tumor hypoxia that can be broadly categorized as either invasive techniques, such as the measurement of oxygen partial pressure (pO_2) with polarographic electrodes and immunohistochemical (IHC) staining of endogenous and/or exogenous markers of hypoxia, or noninvasive techniques, such as positron emission tomography (PET) imaging using radiolabelled hypoxia markers [1,13–16].

Several radiotracers have been developed for PET imaging of tumor hypoxia, including [^{18}F]fluoromisonidazole ([^{18}F]FMISO), [^{18}F] fluoroazomycin arabinoside ([^{18}F]FAZA), 2-(2-nitro-1*H*-imidazol-1-yl)-N-(2,2,3,3,3-[^{18}F]pentafluoropropyl)-acetamide ([^{18}F]EF5) and [^{64}Cu]Cu(II)-diacetyl-bis(N^4-methylthiosemicarbazone) ([^{64}Cu] ATSM), all of which have confirmed the clinical utility of PET hypoxia imaging method in multiple tumor types [17–20]. With the exception of [^{64}Cu]ATSM, these compounds belong to the chemical class of 2- nitroimidazoles (2-NIM), with the key difference being different radiolabel-containing side chain on the imidazole ring in their chemical structure. The variations in ring substituent impart different lipophilicity and thus, differential pharmacokinetic properties to these 2-NIM radiotracers in vivo. 2-NIMs are selectively activated in hypoxic cells through a series of reduction reactions that result in prolonged retention of the reduced species inside the (hypoxic) cell [21]. Members of the 2-NIM class of compounds (pimonidazole and EF5) have also been extensively validated for immunohistochemical detection of hypoxia in tumor biopsies [22–24].

The synthesis of [^{18}F]EF5 was first reported by Dolbier et al. [25]. Preclinical animal studies as well as clinical studies conducted in patients with head and neck cancer and/or glioblastoma established the potential usefulness of [^{18}F]EF5 for PET imaging of tumor hypoxia [19,26–28]. The advantages of [^{18}F]EF5 as a PET hypoxia imaging agent include its uniform tissue distribution characteristics as a result of its higher lipophilicity, high in vivo stability against non-hypoxia mediated metabolism in humans and the unique possibility of assessing hypoxia by immunofluorescence methods upon co-injection of patients with its non-radioactive analogue, EF5 [28,29].

However, the advantages of [^{18}F]EF5 have been somewhat offset by the complexity of its synthesis. [^{18}F]EF5 synthesis is performed by reacting carrier-added [^{18}F]F_2 gas with the trifluoroallyl precursor in trifluoroacetic acid (TFA) (Fig. 1). As only about half of the [^{18}F] activity produced could actually be extracted from the most commonly used target materials for [^{18}F]F_2 production (e.g. Nickel-200, 6061T6 Aluminum) [30], a limited amount of starting radioactivity ([^{18}F]F_2) is available for the radiosynthesis. Further impediment to the synthesis and easier automation of [^{18}F]EF5 is the requirement for solvent (TFA) evaporation and/or work-up procedure prior to its purification by HPLC [25,26,31]. TFA removal generally requires heat-and/or vacuum-assisted evaporation, which is not only time consuming but may also contribute to product decomposition as evidenced by the presence of several peaks on the semi-preparative HPLC chromatogram when the TFA evaporation procedure was used in our experiments, and as indicated by other reports on [^{18}F]EF5 synthesis [25,31,32]. In this study, we have achieved significant improvements in the [^{18}F]EF5 radiosynthesis procedure by employing an electroformed nickel target for production of [^{18}F]F_2 and Oasis cartridges that enabled on-line solid phase extraction (SPE) of the radiotracer and simplification of the purification process [33]. These modifications

now permit the preparation of multiple patient doses of [^{18}F]EF5 starting from relatively low initial activity levels of [^{18}F]F_2, which could greatly facilitate routine production of [^{18}F]EF5 on cyclotrons with a deuteron beam.

2. Materials and methods

2.1. Materials

The radiosynthesis precursor, 2-(2-nitro-1[*H*]-imidazol-1-yl)-*N*-(2,3,3-trifluoroallyl)-acetamide, and nonradioactive EF5 used in this study were provided by Varian Medical Systems (Palo Alto, CA). Reagent grade trifluoroacetic acid was purchased from J.T. Baker (Phillipsburg, NJ), USP ethanol from Tarr Chemical (Portland, OR), ACS/HPLC grade methanol from Burdick & Jackson (Muskegon, MI); sodium hydroxide and disodium hydrogen phosphate were from Sigma-Aldrich (St. Louis, MO) and EM Scientific (Gibbstown, NJ), respectively. High-performance liquid chromatography (HPLC) was performed using a Knauer Model K-501 pump and Knauer Model K- 2501 UV–VIS detector set at 325 nm. Effluent from the UV–VIS detector was coupled to a Carroll & Ramsey Associates Model 105S radiation detector.

2.2. [^{18}F]EF5 synthesis

[^{18}F]F_2 gas was produced via the ^{20}Ne(d, α)^{18}F reaction using a tapered-bore electroformed nickel (Servometer, Cedar Grove NJ) target filled with neon gas containing carrier fluorine that varied between 65 and 90 μmol. Irradiations were conducted using the 15 MeV deuteron beam of a TCC Model CS-30 Cyclotron. The resulting [^{18}F]F_2 gas was bubbled through 3 ml of TFA solution containing the allyl precursor (10 mg; 0.04 mmol) at 0°C with helium as a sweep gas over a period of about 15 min (Fig. 1). Following fluorination, the crude mixture was neutralized by slow addition of 10N NaOH (3 mL) and 0.1 M Na_2HPO_4 buffer (3.6 mL), and transferred via 50–75 psi nitrogen gas onto two pre-conditioned Oasis HLB columns (4.6×20 mm, Waters Corporation, Milford MA) connected in series in place of the injection loop on the semi-preparative (prep) HPLC six-port injection valve (VICI Model 2C6UW) as depicted in Figs. 2 and 3. Just prior to use, the two Oasis columns, stored between runs in acetonitrile, were conditioned with 5 mL of sterile water. When the same addition line was used for both base solutions, 0.5 mL of water followed addition of the NaOH. The Oasis columns were then rinsed by addition of water (3 mL) to the reaction vessel, and repeating the transfer process to purge salts and free fluoride [$^{18}F^-$], if any, present in the crude mixture. Further purification of the [^{18}F]EF5 was done by switching the injector and eluting the contents onto the semi-prep column with the mobile phase. The semi-prep HPLC system consisted of an Eldex Model 1SMP pump, a Waters μBondapack C18 column (10 μm, 7.8×300 mm) and 20% ethanol in water as the mobile phase at a flow rate of 2 ml/min. Elution of the [^{18}F]EF5 peak occurred at about 30 min after transfer to the semi-prep column. Ethanol was evaporated by bubbling nitrogen through the solution at 85 °C. This was followed by sterile filtration of the product through a 0.22 μm membrane filter (Millex GV, Millipore, Billerica, MA) into a sterile vial. The solution was made isotonic using a suitable amount of 14.6% NaCl (Hospira, Inc., Lake Forest, IL). Quality control analysis was performed on an analytical HPLC system (described above) consisting of an Alltima C18 column (5 μm, 4.6×250 mm, Alltech Associates, Deerfield, IL) eluted with 40% methanol in water at a flow rate of 1 ml/min.

2.3. Xenograft tumor model

Animal experiments were conducted according to Institutional Animal Care and Uses Committee (IACUC) regulations and followed a study protocol approved by the IACUC. Human colorectal cancer (HCT116) xenografts were established by subcutaneous injection of 2×10^6 cells suspended in Matrigel (BD Biosciences, Bedford, MA) mixed with

Dulbecco's Modified Eagle Medium (Invitrogen, Carlsbad, CA), into the right hind limb of female nude mice (0.1 mL). The mean body weight of animals on the day of imaging was 27.0±1.9 g. Animals were used for small animal PET imaging when their tumors reached 8–12 mm diameter (n=3).

2.4. Small animal PET imaging

Small animal PET imaging was performed on a microPET R4 system (Concorde Microsystems, Knoxville TN) [34]. Animals were anesthetized using 1.5–2% isoflurane in medical grade air for radiotracer injection and for PET imaging but were left unanesthetized in between, and were allowed to move freely in their cages. Mice were injected with 6.9±0.9 MBq (186±24 μCi) of [^{18}F]EF5 via the tail vein, and static emission scans were acquired for 15–20 min at about 160 min after injection of the radiotracer. After the PET scan, mice were administered with pentobarbital sodium (50 mg/kg i.p.) for induction of deep anesthesia, and the tumor as well as part of the muscle from the opposite leg were collected from each animal. The tissues were weighed and their radioactivity (gamma counts) was measured in an automated gamma counter (Wallac Wizard, Perkin-Elmer, Bridgeville, PA). The gamma counts were normalized for the weight of the tissue to obtain CPMs/g values, and tumor-to-muscle (T/M) ratios were calculated from this data. Small animal PET data were reconstructed for analysis using OSEM3D/MAP reconstruction (2 OSEM3D iterations and 18 MAP iterations) with no corrections applied for attenuation or scatter. Images were analyzed using the ASIPro™ software provided by Concorde Microsystems. Two-dimensional regions of interest (2D ROIs) were drawn on transaxial planes covering the entire tumor area and muscle region on the opposite leg. The ^{18}F activity counts in the reconstructed images were converted to concentration values (nCi/cc) by applying a system calibration factor that was derived from imaging a mouse-size syringe filled with water containing a known concentration of ^{18}F. For each animal, the measured tissue activity concentrations (mean of all ROIs) were expressed as percentage injected dose per gram tissue (% ID/g), mean standard uptake value (SUV_{mean}) and T/M ratio.

3. Results

Targetry and cyclotron production of [^{18}F]F_2

For 18 irradiations using the electroformed nickel target at 14.9± 1.5 μA for 108±15 min, the total amount of ^{18}F activity recovered at end-of-bombardment (EOB) was 16.2±2.2GBq (438±58 mCi). Correcting for degradation of beam energy through a 50 μmCu/Be foil, an 85% transmission edge-cooled aluminum grid and IAEA recommended yields for the (d,α) reaction on natural Ne (91.8 mCi/uA at the calculated energy of 13.6 MeV [35]) indicated that the recovery of the ^{18}F produced in the target was about 76%.

3.2. Radiosynthesis of [^{18}F]EF5

The amount of [^{18}F]EF5 collected at the end-of synthesis (EOS) was 1140±200 MBq (30.8±5.4 mCi), and ranged from 755–1465 MBq (20.4–39.6 mCi; n=18). The synthesis time was about 75 minutes, including [^{18}F]F_2 bubbling (12–15 min), neutralization, Oasis SPE (12–15 min) and further purification by HPLC (~35 min). The EOB radiochemical yield, calculated from the total amount of post-irradiation ^{18}F activity recovered at different stages of the synthesis, i.e., unreacted [^{18}F]F_2 trapped in soda lime, radioactivity recovered from Oasis and HPLC eluates, and the [^{18}F]EF5 product peak, was found to be 11±2% (n=18). The chemical and radiochemical purity of the formulation was found to be ≥;98%. The specific radioactivity was determined to be 327±95 MBq/μmol (8.83±2.58 mCi/μmol) and ranged from 165.8–454 MBq/μmol (4.48–12.27 mCi/μmol). The identity of the compound was confirmed by comparing its retention time to that of the cold standard (t_R=10.5–14.0 min). Additionally, LC/MS analysis was performed on final formulations

(n=2) after radioactivity decay, and showed a single major peak with m/z 303.0 corresponding to EF5 ($[M+H]^+$, theoretical m/z: 303.2). The pH of the formulation was also measured after the decay of the radioactivity and was consistently neutral.

3.3. Functional assessment of [^{18}F]EF5 in vivo

The mean tumor volume on the day of imaging experiments was 458±9 mm^3(n=3). The percentage of injected [^{18}F]EF5 accumulated per gram tissue (% ID/g) for individual tumors at about 160 minutes post-injection were 1.01, 1.66 and 1.00, and the mean SUV values (SUV_{mean}) were 0.29, 0.42, and 0.27, respectively (Table 2). The mean T/M ratio calculated from small animal PET images was 2.71±0.31 compared to 3.18±0.48 from ex vivo gamma counting.

4. Discussion

In general, target bodies for production of [^{18}F]F_2 are made from Inconel, Nickel-200 or 6061T6 Aluminum [30]. The initial tapered-bore target for [^{18}F]F_2 production used in this work was made from 6061 T6 aluminum; however, as only 50% of the [^{18}F]F_2 gas was recovered from aluminum or Ni-200 [30], an electroformed nickel tapered-bore target was fabricated (Bruce Technologies, Chapel Hill, NC) and utilized. High strength, high purity electroformed nickel has been previously suggested as a target body material for PET radionuclide production [36]. However, the use of relatively large volume, cylindrical bore electroformed Ni targets for [^{18}F]F_2 production met with limited success in terms of percent ^{18}F recovered [37]. Results for the use of a small volume, tapered-bore electroformed Ni target [30] for [^{18}F]F_2 production led to the modified design used herein. The target body and mating cooling jacket geometries were designed to maximize heat transfer. This was accomplished by maximizing both the surface area of the external convective boundary and the convective heat transfer coefficient. The flow regime within the cooling jacket is fully developed turbulent, thus the convective heat transfer coefficient is maximized by selecting channel dimensions (within practical limits) that yield the largest Reynolds number [38].

[^{18}F]EF5 was synthesized by reacting gaseous [^{18}F]F_2 with the trifluoroallyl precursor dissolved in TFA following the first report by Dolbier et al. [25]. Several improvements have been recently reported for the synthesis of [^{18}F]EF5, for example, a significant increase in [^{18}F] F_2 incorporation and EF5 yield (vs. cold precursor) were observed by Kachur et al. when catalytic amounts of iodine were used in the reaction [32]. Also, Eskola et al. have reported on [^{18}F]EF5 synthesis using relatively high specific activity [^{18}F]F_2 prepared via an electrical discharge method starting from conventional nucleophilic fluoride ([$^{18}F^-$]) [31]. This method provided on average 595 MBq (16.08 mCi) of [^{18}F]EF5 at EOS with a starting [^{18}F]F^- radioactivity of 37 GBq (1 Ci). For comparison, the reaction conditions and radiochemical yields for [^{18}F]EF5 production reported in the literature are summarized in Table 1. With goals of increasing the amount of purified [^{18}F]EF5 collected at EOS for our preclinical imaging studies plus simplification of the purification process, we developed a new procedure that eliminates the need for potentially detrimental vacuum and/or heat assisted solvent (TFA) evaporation prior to HPLC purification. This new method enabled us to collect about 1140 MBq (30.8 mCi) of [^{18}F] EF5 starting from about 16.2 GBq (438 mCi) of [^{18}F]F_2, which represents an approximately 4-fold improvement compared with the method of Eskola et al. [31]. The higher amounts combined with the simplified purification process presented in this work allow for reliable production and supply of [^{18}F]EF5 in multiple patient doses as required for its clinical utility.

After the radiolabeling reaction, the TFA solvent was partially neutralized with the use of sodium hydroxide and phosphate buffer, and the crude product was pre-purified by passage

through two Oasis on-line solid phase extraction (SPE) columns connected to the semi-preparative HPLC system. Final purification of the product was achieved by eluting the compounds from Oasis cartridges onto the semi-preparative column. Unpredictable and excessive evaporation of TFA by helium and/or neon during $[^{18}F]F_2$ bubbling may cause a shift in pH of the reaction mixture to basic conditions when neutralization is attempted with sodium hydroxide. For this reason, $[^{18}F]F_2$ bubbling was carried out at 0 °C to have minimal and reproducible evaporation of TFA among syntheses. In addition, the pH of the crude mixture was maintained in acidic conditions by achieving near- but not complete-neutralization to have a precipitate- free solution prior to its loading on to the Oasis columns. Fig. 4 shows comparative semi-prep HPLC chromatograms of $[^{18}F]$EF5 made via the reported TFA evaporation method and the new on-line SPE method used in this work. As can be seen in these chromatograms, several large peaks were present in the HPLC chromatogram (UV) when the TFA solvent was removed by distillation followed by resolubilization of the crude product in water at elevated temperature prior to injection onto the HPLC. This suggests a possible decomposition of the precursor and/or the $[^{18}F]$EF5 during the evaporation process, in addition to the side products that are generated during the $[^{18}F]F_2$ bubbling. In contrast, EF5 was the only major peak observed in the elution time window when the crude mixture was neutralized using 10N NaOH and pre-purified using the Oasis method described herein. Additionally, previous reports on $[^{18}F]$EF5 synthesis have indicated the presence of free fluoride ($^{18}F^-$) and other hydrophilic labeled side products in the crude reaction mixture. As these products are minimally extracted by the Oasis stationary phase, they can be easily removed from the crude mixture by passage through the Oasis HLB columns prior to HPLC purification.

In order to evaluate the leakage of $[^{18}F]$EF5 through the Oasis columns during the SPE, the Oasis eluate as well as the water rinse fraction were analyzed using analytical HPLC following each synthesis and after decay of the radioactivity. The analyses always showed varying amounts of EF5 breakthrough when a single Oasis cartridge was used for the purification. This is most likely due to sample overload (10 mg) on a relatively small size column (4.6×20 mm) and because of the protonated state of EF5 as well as other imidazole-containing side products in the acidic pH of the crude mixture. The unretained fraction of EF5 varied among syntheses and, in general, increased as the number of syntheses performed on the column increased. As much as 32% of the total measured EF5 was found in the eluate after 10–15 syntheses when a single cartridge was used. We were able to solve this problem by employing two Oasis cartridges connected in series; no breakthrough of $[^{18}F]$EF5 was observed even after 11 consecutive syntheses using the same columns. Also, the use of two Oasis columns did not cause any significant increase in back pressure for semi-preparative HPLC. In our method, we utilized the minimum amount of carrier F_2 gas that yielded the highest reproducible $[^{18}F]F_2$ output from the cyclotron target. As a result, we have about 1.5- to 2.2-fold excess of the carrier fluorine gas for the reaction (65–90 μmol vs. 40 μmol precursor), which is comparable to other reports on $[^{18}F]$EF5 using the low specific activity $[^{18}F]F_2$ [Table 1]. However, it is evident from our semi-preparative HPLC chromatograms that most of the radiolabelling precursor is consumed in the reaction, and this suggests that it may be possible to further improve the radiochemical yield vs. starting $[^{18}F]F_2$ by increasing the amount of precursor and/or further reducing the amount of carrier fluorine. The specific radioactivity of $[^{18}F]$EF5 synthesized in this work was found to be about 327 MBq/μmol (8.83 mCi/μmol). This is about 3-fold higher than that presented by Apte et al. [39] but 20-fold lower than that achieved by Eskola et al. using moderately high specific activity $[^{18}F]F_2$ [31]. Based on the specific radioactivity obtained in this work and assuming a maximum dose of 370 MBq (10 mCi) of $[^{18}F]$EF5 for human PET studies, we anticipate that we would have approximately 0.5 mg of EF5 present in each dose for patients. For comparison, less than 15 μg of nonradioactive compound is reported to be present in patient doses for other clinically used ^{18}F-labeled hypoxia imaging agents, for

example, [^{18}F]FMISO and [^{18}F]FAZA [15,40], both of which are synthesized via no-carrier-added nucleophillic radiofluorination yielding high specific radioactivity formulations for these tracers. However, as the reduction and binding of EF5, and 2-nitroimidazole hypoxia markers in general, is dependent on cellular O_2 concentration and the activating nitroreductase enzymes [15,41], the specific radioactivity achieved to date should be acceptable for PET imaging of tumor hypoxia with labeled nitroimidizole tracers. Additionally, specific activity measurements revealed that the whole body concentration of nonradioactive EF5 that animals received from [^{18}F]EF5 dose during small animal PET imaging experiments in this study was only about 12 μM as compared to the standard dose of 100 μM (3.6 vs. 30.2 mg/kg body weight) used for immunofluorescence detection of hypoxic cells with EF5 [42].

As an indicator of the functional activity of [^{18}F]EF5 synthesized via the modified procedure, small animal PET imaging of nude mice bearing human colon cancer xenografts (n=3) was performed. Imaging was performed at about 160 min after injection of animals with [^{18}F]EF5 and by following previous reports [19,26], which showed 2–3 h postinjection as the optimal time period for measuring hypoxia-specific binding of [^{18}F]EF5 with PET. Using endogenous and exogenous markers of hypoxia, carbonic anhydrase 9 and pimonidazole, respectively, we have previously shown that subcutaneous tumors grown from this tumor line (HCT116) are hypoxic [43,44]. In these studies, the fraction of tumor that is positive for pimonidazole binding was found be >20%, indicating the severity of hypoxia in this tumor type. Consistent with the hypoxic nature of this xenograft, all three animals imaged in the current study showed high accumulation of [^{18}F]EF5 in tumors, with T/M ratios ranging from 2.5–3.1 on PET images (Fig. 5, Table 2). The uptake of [^{18}F]EF5 in tumors was confirmed by gamma counting of tumor and muscle tissue isolated from opposite leg of the same animal after small animal PET imaging. The differences in animal models, tumor type and variations in study time periods makes it difficult to compare the tumor uptake and normal tissue retention of [^{18}F]EF5 observed in this study with those reported in the literature for this radiotracer and/or other widely used 2-nitroimidazole radiotracers. Nevertheless, comparison of % ID/g value derived from ex-vivo gamma counting for the muscle tissue in the present study as well as that reported by Eskola et al. for [^{18}F]EF5 (0.55 and 0.38, respectively) with the values for two extensively studied hypoxia imaging agents, [^{18}F]FMISO and [^{18}F]FAZA, revealed that the clearance of background radioactivity from the muscle tissue is similar for [^{18}F]EF5 and [^{18}F]FAZA (0.55 and 0.38 at 2–3 h vs. 0.26–0.65 for [^{18}F]FAZA at 3 h) but is significantly slower for [^{18}F]FMISO (% ID/g 0.79–1.26 at 3 h) [31,45,46]. Consistent with these observations, the uptake of [^{18}F]EF5 in HCT116 tumors (% ID/g: 1.68±0.28) in our study is comparable to the uptake levels reported for [^{18}F]FAZA with % ID/g values 1.35±0.89, 1.38±0.62, 2.96±1.27 in AR42J, EMT6 and A431 xenografts, respectively, whereas the uptake levels of [^{18}F]FMISO in the same tumor models were reported to be significantly higher than for [^{18}F]FAZA albeit with significantly lower tumor-to-muscle ratios at 3 h after injection [45]. Additionally, the tumor and muscle SUVs of 0.33±0.08 and 0.12±0.04 derived from PET images for [^{18}F]EF5 in the present study are very similar to [^{18}F]FAZA SUVs of 0.35±0.12 and 0.13±0.05 reported by Sorger et al. in a Walker 256 tumor bearing rat model [47]. Taken together, these data suggest that [^{18}F]FAZA and [^{18}F]EF5 might possess comparable in vivo characteristics and tumor uptake levels despite the difference in their lipophilicity (partition coefficient of 1.1 for FAZA vs. 5.5 for EF5 [15,46]), and warrants further investigation for direct comparison of these two tracers in the same tumor type.

5. Conclusion

A simple procedure has been developed for the routine synthesis of [^{18}F]EF5 in amounts and purity required for clinical studies. For example, our data demonstrate that with an

electroformed nickel target, a 120-min irradiation with 15 μA of 7–9 MeV deuterons, in concert with the methods detailed herein, should routinely provide 370–740 MBq (10–20 mCi) of [^{18}F]EF5 at EOS. Moreover, this new method also enables facile automation of the synthesis using commercially available radiosynthesis modules.

Acknowledgments

This work was supported by research grants from Varian Medical Systems and the NIH (CA42324 and CA40355). We thank Dr. G. Allan Johnson for his support on the use of small animal PET scanner; Shawn Murphy and Michael Dailey for their assistance in the preparation of [^{18}F]F_2.

References

1. Vaupel P, Hoeckel M, Mayer A. Detection and characterization of tumor hypoxia using pO_2 histography. Antioxid Redox Signal. 2007; 9:1221–35. [PubMed: 17536958]
2. Brizel DM, Sibley GS, Prosnitz LR, Scher RL, Dewhirst MW. Tumor hypoxia adversely affects the prognosis of carcinoma of the head and neck. Int J Radiat Oncol Biol Phys. 1997; 38:285–9. [PubMed: 9226314]
3. Semenza GL. Hypoxia, clonal selection, and the role of HIF-1 in tumor progression. Crit Rev Biochem Mol Biol. 2000; 35:71–103. [PubMed: 10821478]
4. Harris AL. Hypoxia — a key regulatory factor in tumour growth. Nat Rev Cancer. 2002; 2:38–47. [PubMed: 11902584]
5. Pennacchietti S, Michieli P, Galluzzo M, Mazzone M, Giordano S, Comoglio PM. Hypoxia promotes invasive growth by transcriptional activation of the met protooncogene. Cancer Cell. 2003; 3:347–61. [PubMed: 12726861]
6. Papandreou I, Cairns RA, Fontana L, Lim AL, Denko NC. HIF-1 mediates adaptation to hypoxia by actively downregulating mitochondrial oxygen consumption. Cell Metab. 2006; 3:187–97. [PubMed: 16517406]
7. Gort EH, Groot AJ, van der Wall E, van Diest PJ, Vooijs MA. Hypoxic regulation of metastasis via hypoxia-inducible factors. Curr Mol Med. 2008; 8:60–7. [PubMed: 18289014]
8. Rofstad EK, Sundfor K, Lyng H, Trope CG. Hypoxia-induced treatment failure in advanced squamous cell carcinoma of the uterine cervix is primarily due to hypoxia-induced radiation resistance rather than hypoxia-induced metastasis. Br J Cancer. 2000; 83:354–9. [PubMed: 10917551]
9. Tredan O, Galmarini CM, Patel K, Tannock IF. Drug resistance and the solid tumor microenvironment. J Natl Cancer Inst. 2007; 99:1441–54. [PubMed: 17895480]
10. Shannon AM, Bouchier-Hayes DJ, Condron CM, Toomey D. Tumour hypoxia, chemotherapeutic resistance and hypoxia-related therapies. Cancer Treat Rev. 2003; 29:297–307. [PubMed: 12927570]
11. Graeber TG, Osmanian C, Jacks T, Housman DE, Koch CJ, Lowe SW, et al. Hypoxia-mediated selection of cells with diminished apoptotic potential in solid tumours. Nature. 1996; 379:88–91. [PubMed: 8538748]
12. Gottesman MM, Fojo T, Bates SE. Multidrug resistance in cancer: role of ATP-dependent transporters. Nat Rev Cancer. 2002; 2:48–58. [PubMed: 11902585]
13. Vordermark D, Brown JM. Endogenous markers of tumor hypoxia — predictors of clinical radiation resistance? Strahlentherapie Und Onkologie. 2003; 179:801–11. [PubMed: 14652668]
14. Ljungkvist ASE, Bussink J, Kaanders J, Van der Kogel AJ. Dynamics of tumor hypoxia measured with bioreductive hypoxic cell markers. Radiat Res. 2007; 167:127–45. [PubMed: 17390721]
15. Krohn KA, Link JM, Mason RP. Molecular imaging of hypoxia. J Nucl Med. 2008; 49:129S–48S. [PubMed: 18523070]
16. Bussink J, Kaanders J, van der Kogel AJ. Tumor hypoxia at the micro-regional level: clinical relevance and predictive value of exogenous and endogenous hypoxic cell markers. RadiotherOncol. 2003; 67:3–15.

17. Lee ST, Scott AM. Hypoxia positron emission tomography imaging with ^{18}F-fluoromisonidazole. Semin Nucl Med. 2007; 37:451–61. [PubMed: 17920352]
18. Postema EJ, McEwan AJB, Riauka TA, Kumar P, Richmond DA, Abrams DN, et al. Initial results of hypoxia imaging using 1-alpha-D-(5-deoxy-5-^{18}F-fluoroarabino-furanosyl)- 2-nitroimidazole (^{18}F-FAZA). Eur J Nucl Med Mol Imaging. 2009; 36:1565–73. [PubMed: 19430784]
19. Komar G, Seppanen M, Eskola O, Lindholm P, Gronroos TJ, Forsback S, et al. ^{18}F-EF5: a new PET tracer for imaging hypoxia in head and neck cancer. J Nucl Med. 2008; 49:1944–51. [PubMed: 18997048]
20. Dehdashti F, Grigsby PW, Mintun MA, Lewis JS, Siegel BA, Welch MJ. Assessing tumor hypoxia in cervical cancer by positron emission tomography with ^{60}Cu-ATSM: relationship to therapeutic response — a preliminary report. Int J Radiat Oncol Biol Phys. 2003; 55:1233–8. [PubMed: 12654432]
21. Nunn A, Linder K, Strauss HW. Nitroimidazoles and imaging hypoxia. Eur J Nucl Med Mol. 1995; 22:265–80.
22. Kaanders JH, Wijffels KI, Marres HA, Ljungkvist AS, Pop LA, van den Hoogen FJ, et al. Pimonidazole binding and tumor vascularity predict for treatment outcome in head and neck cancer. Cancer Res. 2002; 62:7066–74. [PubMed: 12460928]
23. Evans SM, Fraker D, Hahn SM, Gleason K, Jenkins WT, Jenkins K, et al. EF5 binding and clinical outcome in human soft tissue sarcomas. Int J Radiat Oncol Biol Phys. 2006; 64:922–7. [PubMed: 16458778]
24. Evans SM, Judy KD, Dunphy I, Jenkins WT, Hwang WT, Nelson PT, et al. Hypoxia is important in the biology and aggression of human glial brain tumors. Clin Cancer Res. 2004; 10:8177–84. [PubMed: 15623592]
25. Dolbier WR, Li AR, Koch CJ, Shiue CY, Kachur AV. ^{18}F-EF5, a marker for PET detection of hypoxia: synthesis of precursor and a new fluorination procedure. Appl Radiat Isotopes. 2001; 54:73–80.
26. Ziemer LS, Evans SM, Kachur A, Shuman AL, Cardi CA, Jenkins WT, et al. Noninvasive imaging of tumor hypoxia in rats using the 2-nitroimidazole ^{18}F-EF5. Eur J Nucl Med Mol. 2003; 30:259–66.
27. Koch CJ, Shuman AL, Jenkins WT, Kachur AV, Karp JS, Freifelder R, et al. The radiation response of cells from 9L gliosarcoma tumours is correlated with ^{18}F-EF5 uptake. Int J Radiat Oncol Biol Phys. 2009; 85:1137–47.
28. Koch CJ, Scheuermann JS, Divgi C, Judy KD, Kachur AV, Freifelder R, et al. Biodistribution and dosimetry of ^{18}F-EF5 in cancer patients with preliminary comparison of ^{18}F-EF5 uptake versus EF5 binding in human glioblastoma. Eur J Nucl Med Mol. 2010; 37:2048–59.
29. Koch CJ, Hahn SM, Rockwell K, Covey JM, McKenna WG, Evans SM. Pharmacokinetics of EF5 2-(2-nitro-1-H-imidazol-1-yl)-N-(2,2,3,3,3-pentafluoropropyl) acetamide in human patients: implications for hypoxia measurements in vivo by 2-nitrolmidazoles. Cancer Chemother Pharmacol. 2001; 48:177–87. [PubMed: 11592338]
30. Bishop A, Satyamurthy N, Bida G, Phelps M, Barrio JR. Metals suitable for fluorine gas target bodies: first use of aluminum for the production of [^{18}F]F_2. Nucl Med Biol. 1996; 23:181–8. [PubMed: 8782225]
31. Eskola O, Grönroos TJ, Forsback S, Tuomela J, Komar G, Bergman J, et al. Tracer level electrophilic synthesis and pharmacokinetics of the hypoxia tracer [^{18}F]EF5. Mol Imaging Biol. 2011
32. Kachur AV, Dolbier WR Jr, Xu W, Koch CJ. Catalysis of fluorine addition to double bond: an improvement of method for synthesis of ^{18}F PET agents. Appl Radiat Isotopes. 2010; 68:293–6.
33. Chitneni S, Bida G, Dewhirst M, Zalutsky M. A simplified synthesis of the hypoxia imaging agent 2-(2-Nitro-1H-imidazol-1-yl)-N-(2,2,3,3,3-[^{18}F]pentafluoropropyl)- acetamide([^{18}F]EF5). J Nucl Med. 2011; 52(Supp 1):1428.
34. Knoess C, Siegel S, Smith A, Newport D, Richerzhagen N, Winkeler A, et al. Performance evaluation of the microPET R4 PET scanner for rodents. Eur J Nucl Med Mol Imaging. 2003; 30:737–47. [PubMed: 12536244]

35. Diagnostic radioisotopes and monitor reactions. Vienna: 2001. Charged particle cross-section database for medical radioisotope production. IAEA-TECDOC-1211see also updated information at www-nds.iaea.org/medical/
36. Wieland BW, Fowler JS, Wolf AP. Multi-purpose target unit for small cyclotrons. J Label Cmpds Radiopharm. 1984; 21:1250–1.
37. Dahl, JR.; Belakhlef, A.; Matacchieri, RA.; Chaly, TC.; Koziorowski, J.; Margouleff, D. A target for the routine production of [^{18}F]-F_2. In: Dahl, JR.; Ferrieri, R.; Finn, R.; Schlyer, DJ., editors. Proc of the Vth International Workshop on Targetry and Target Chemistry. Upton, New York: Brookhaven National Laboratory; 1994. p. 219
38. El-Wakil, MM. Nuclear heat transport. Scranton (Pa): International Textbook Co; 1971.
39. Apte SD, Chin FT, Loo BW, Chang D, Graves EE. An efficient protocol for the radiosynthesis of clinical grade ^{18}F-EF5. J Label Compd Radiopharm. 2011; 54:S408.
40. Souvatzoglou M, Grosu AL, Roper B, Krause BJ, Beck R, Reischl G, et al. Tumour hypoxia imaging with [^{18}F]FAZA PET in head and neck cancer patients: a pilot study. Eur J Nucl Med Mol Imaging. 2007; 34:1566–75. [PubMed: 17447061]
41. Wang J, Foehrenbacher A, Su J, Patel R, Hay MP, Hicks K, et al. The 2-nitroimidazole EF5 is a biomarker for oxidoreductases that activate the bioreductive prodrug CEN-209 under hypoxia. Clin Cancer Res. 2011:1684–95. [PubMed: 22167409]
42. Evans SM, Joiner B, Jenkins WT, Laughlin KM, Lord EM, Koch CJ. Identification of hypoxia in cells and tissues of epigastric 9L rat glioma using EF5 [2-(2-nitro-lH-imidazol-1-yl)-*N*-(2,2,3,3,3-pentafluoropropyl) acetamide]. Br J Cancer. 1995; 72:875–82. [PubMed: 7547234]
43. Cao Y, Li CY, Moeller BJ, Yu D, Zhao Y, Dreher MR, et al. Observation of incipient tumor angiogenesis that is independent of hypoxia and hypoxia inducible factor-1 activation. Cancer Res. 2005; 65:5498–505. [PubMed: 15994919]
44. Cao Y, Sonveaux P, Liu S, Zhao Y, Mi J, Clary BM, et al. Systemic overexpression of angiopoietin-2 promotes tumor microvessel regression and inhibits angiogenesis and tumor growth. Cancer Res. 2007; 67:3835–44. [PubMed: 17440098]
45. Piert M, Machulla HJ, Picchio M, Reischl G, Ziegler S, Kumar P, et al. Hypoxia-specific tumor imaging with ^{18}F-fluoroazomycin arabinoside. J Nucl Med. 2005; 46:106–13. [PubMed: 15632040]
46. Reischl G, Dorow DS, Cullinane C, Katsifis A, Roselt P, Binns D, et al. Imaging of tumor hypoxia with [^{124}I]IAZA in comparison with [^{18}F]FMISO and [^{18}F]FAZA–first small animal PET results. J Pharm Pharm Sci. 2007; 10:203–11. [PubMed: 17706178]
47. Sorger D, Patt M, Kumar P, Wiebe LI, Barthel H, Seese A, et al. [^{18}F] Fluoroazomycinarabinofuranoside (^{18}FAZA) and [^{18}F]Fluoromisonidazole (^{18}FMISO): a comparative study of their selective uptake in hypoxic cells and PET imaging in experimental rat tumors. Nucl Med Biol. 2003; 30:317–26. [PubMed: 12745023]

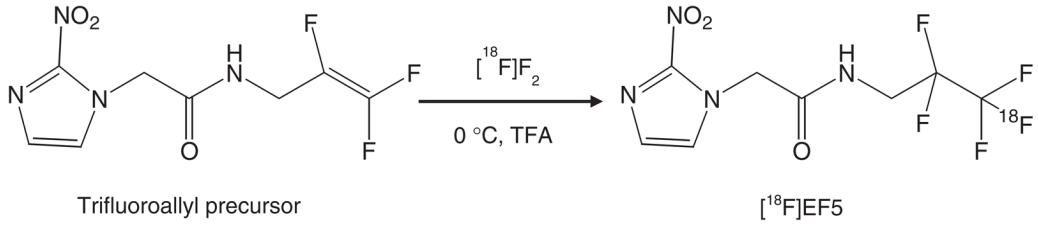

Fig. 1.
Synthesis of [^{18}F]EF5 starting from its allyl precursor and by using [^{18}F]F_2 gas in trifluoroacetic acid solvent.

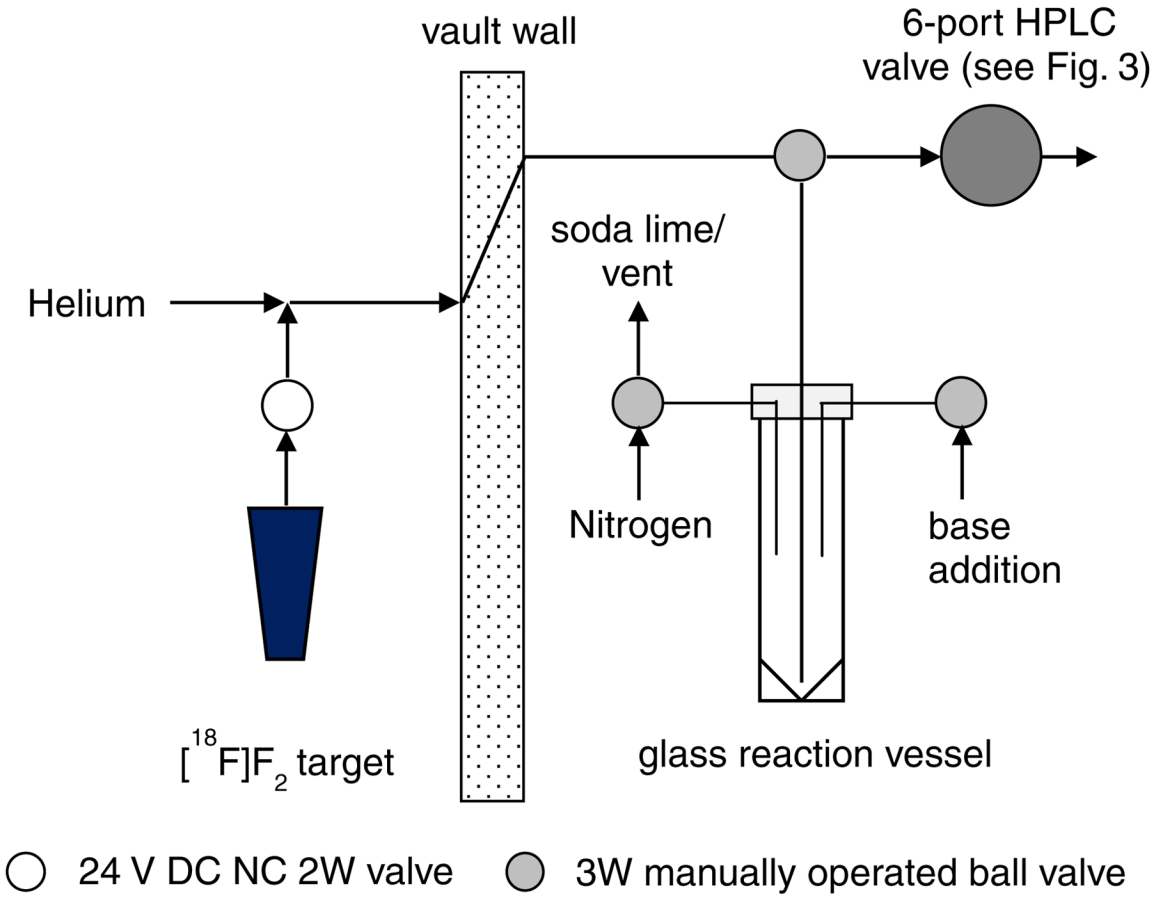

Fig. 2.
Schematic representation of the apparatus and synthesis setup used for the preparation of [^{18}F]EF5.

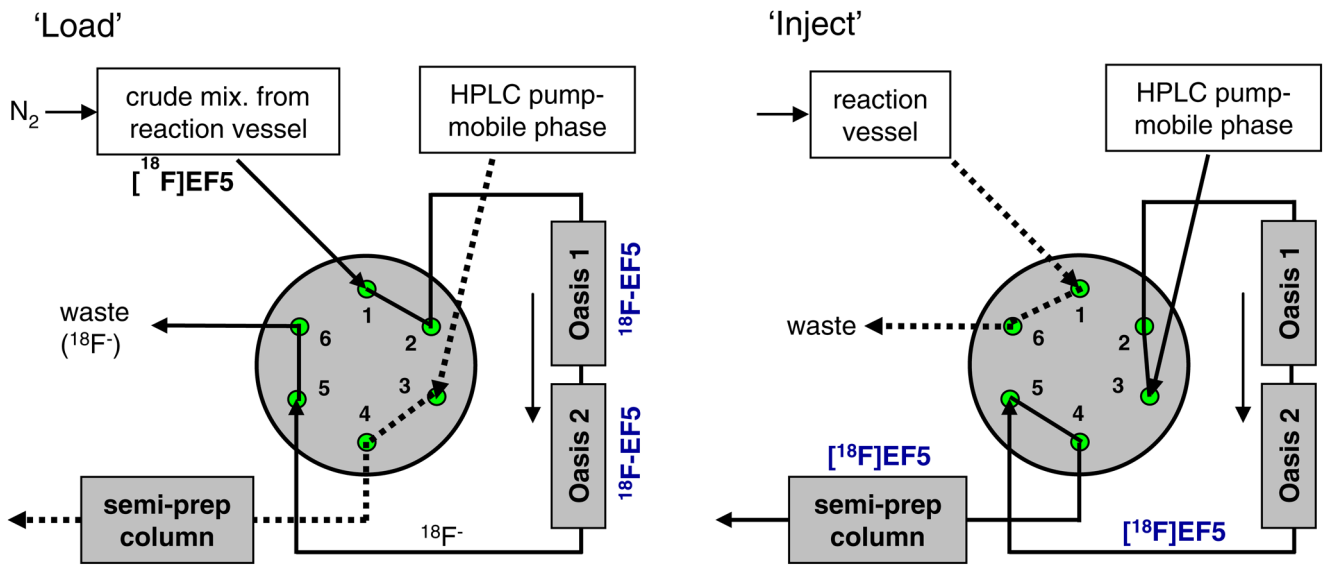

Fig. 3.

HPLC configuration for the purification of [^{18}F]EF5 using Oasis HLB columns (4.6×20 mm) and the semi-preparative HPLC system. The crude reaction mixture was initially passed through Oasis cartridges (n=2 in series) connected in place of injection loop on the HPLC injector in "load" position (left panel). Further purification was achieved by switching the injector to "inject" position and eluting the contents onto the semi-prep column (right panel).

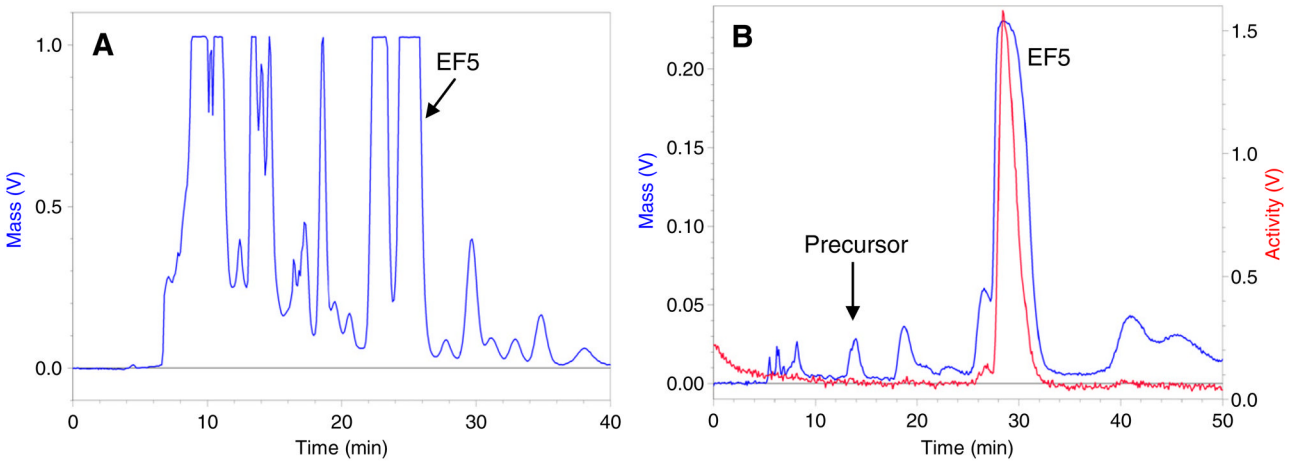

Fig. 4.

Comparative semi-prep HPLC chromatograms of [^{18}F]EF5 prepared via the TFA evaporation method (A) and the new Oasis method (B). EF5 was the major peak present in the elution time window for the Oasis method as opposed to several large peaks observed in the TFA evaporation method.

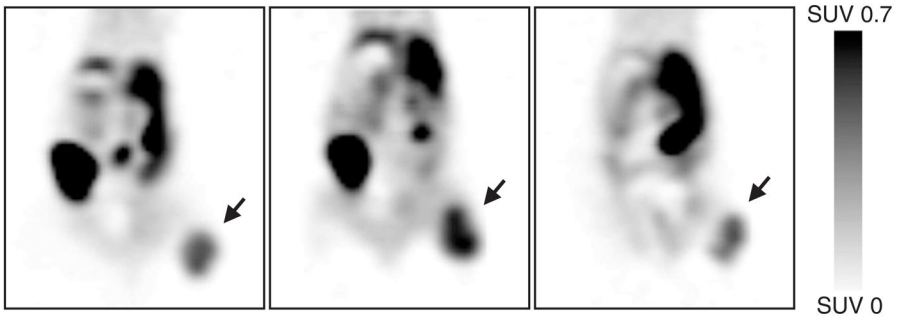

Fig. 5.

[^{18}F]EF5 PET images of athymic nude mice bearing HCT116 tumors on their lower right limb (subcutaneous). Images were acquired for 15–20 min at about 160 min after injection of animals with 5.9, 7.5 and 7.2 MBq [^{18}F]EF5, respectively, under isoflurane anesthesia. Images are scaled to the same SUV value for all the three animals and are shown in coronal planes at mid-tumor level. The tumors are indicated by arrows, and an intense accumulation of [^{18}F]EF5 is also seen in the hepatobiliary system as a result of its excretion.

Table 1

Overview of synthesis methods and results for [^{18}F]EF5 as reported in the literature and from the present work.

	Precursor in mg (μmol)	TFA (ml)	Carrier F_2 (μmol)	TFA removal prior to HPLC purification	MBq [^{18}F]EF5 at EOS (mCi)	Radiochemical yield (%)	Specific activity (MBq/μmol)
Dolbier et al. [25]	25 (100)	5	66.7	Neutralization/liquid-liquid extraction/evaporation	NA	>10	NA
Kachur et al. [32]	6–8 (24–32)	8	60–70	Evaporation	NA	NA	NA
Eskola et al. [31]	1–1.2 (4–4.5)	0.6–0.7	0.3–1.2	Evaporation	406–1027 (10.9–27.7)	2.8±0.6[a] (n=19)	6600±1900
Apte et al. (abstract) [39]	22 (88)	7	NA	Evaporation	444–518 (12–14)	4.7[b] (n=8)	67–122
Current work	10 (40)	3	65–90	Neutralization/online-SPE	755–1465 (20.4–39.6)	11±2[a] (n=18)	327±95

NA: Not Available.

[a] EOB.

[b] EOS.

Table 2

% ID/g values, mean SUV values and tumor-to-muscle (T/M) ratios for [^{18}F]EF5 calculated from PET images in comparison with the data obtained from gamma counting for tumor and muscle tissue for each animal.

Animal no.	Tissue	% ID/g		SUV		Tumor-to-muscle ratio	
		Small animal PET	Gamma counting	Small animal PET	Gamma counting	Small animal PET	Gamma counting
1	Tumor	1.01	1.46	0.29	0.42	3.07	3.58
	Muscle	0.33	0.41	0.10	0.12		
2	Tumor	1.66	2.00	0.42	0.51	2.50	2.64
	Muscle	0.67	0.76	0.17	0.19		
3	Tumor	1.00	1.59	0.27	0.42	2.56	3.31
	Muscle	0.39	0.48	0.10	0.13		
Mean±SD	Tumor	1.22±0.38	1.68±0.28	0.33±0.08	0.45±0.05	2.71±0.31	3.18±0.48
	Muscle	0.46±0.18	0.55±0.18	0.12±0.04	0.15±0.04		

Nucl Med Biol. Author manuscript; available in PMC 2012 October 23.